A Novel Two-Phase Permanent Magnet Rotor Machine for Automotive Applications

A Novel Two-Phase Permanent Magnet Rotor Machine for Automotive Applications

Matias F. Troncoso C., Fausto Stella and Gianmario Pellegrino, *Fellow, IEEE*

Abstract – This paper presents a study of permanent magnet machines for automotive applications, comparing different slot, pole and phase number combinations in terms of torque and power output and NVH performance under constraint of the same active volume. FEM simulations are used to estimate electromagnetic performance and an analytical model to evaluate noise emissions for each configuration. In this analysis, a novel two-phase machine with mildly overlapped windings emerges as the best combination between NVH and electromagnetic performance, at the expense of a 4-leg power converter instead of a standard 3-phase 2-level inverter.

Index Terms **– Two-phase, AC Machines, Brushless machines, Electric Machines, Permanent magnet machines**

I. INTRODUCTION

Fractional slot PM machines with concentrated windings are known for short end-windings and overall axial compactness, added to high torque density. For this reason, they are widely employed in applications with high power density requirements such as automotive. In addition, concentrated windings allow modularity and thus simplification of the production phase and high slot fill factors. A typical downside of these motors is the low-order mode vibrations induced by radial and tangential electromagnetic pull, which has been extensively studied [1-3]. The rule of good engineering in this respect is to avoid slot/pole combinations generating low-order modes (such as 12s/10p or 9s/10p), as precise simulation of noise emission is a complicated task.

This paper presents a comparative analysis for concentrated winding motors, elaborated in terms of performance and noise emission for an automotive application, considering different stator windings for the same surface mounted permanent magnet rotor. Table I presents the combinations under study; the table includes the unconventional 20 slot - 10 pole two phase machine, which will be proposed for its performance's benefits for this application. Two-phase machines have been studied for similar applications [4-7]. In [4] is found that both two and three phase applications produce similar torque density and efficiency, but two phases present higher torque ripple.

This paper further expands this comparison by taking into consideration mild overlapped winding (q=2), which makes it possible to achieve unity winding factor with short end-windings and thus obtain higher torque density.

Table I – Motor topologies under comparison

Slot / Pole	9s / 10p	12s / 10p	15s / 10p	20s/10p
Number of phases	3	3	3	2
Winding Layer	Double Layer	Double Layer	Double Layer	Double Layer
Winding Topology	Fractional Slot	Fractional Slot	Fractional Slot	Integer Slot
Winding Throw	1	1	1	2 (overlapped)

In addition, as confirmed by calculation in [5] a two phase machine operated with two full-bridges with respect to a traditional three phase system delivers approximately 15% more of power, by adding an additional inverter leg. Similar performance analysis is performed in [6] where a 2-phase 8slot-10pole is compared with a 3-phase 10slot-10pole machine and showed that 2-phase has higher torque density.

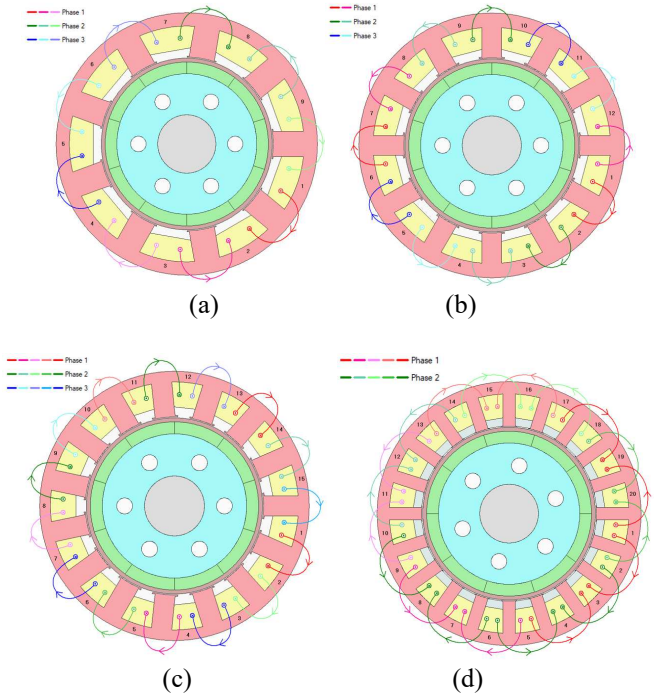

Figure 1. Cross section of the motors under comparison. (a): 9slot – 10 pole. (b) 12 slot – 10 pole. (c) 15 slot – 10 pole. (d) 20 slot – 10 pole.

This work was supported by the Power Electronics Innovation Center (PEIC) of Politecnico di Torino.

M. F. Troncoso and G. Pellegrino are with the Department of Energy, Politecnico di Torino, Turin 10129, Italy. (e-mail: matias.troncoso@polito.it; gianmario.pellegrino@polito.it)

The literature on two-phases remains scarce, probably because of the power converter of increased part count. Its benefits, regarding performance and noise emission, have not yet been widely studied.

II. MACHINES UNDER STUDY

Fig. 1 presents the different stators and windings for the slot-pole combinations under investigation. As can be seen, the winding for 20s10p is overlapped with a pitch of two slots. This results in the coils being full pitched, covering a mechanical angle of 36° equal to one rotor pole pitch. The downsides are longer end windings and loss of modularity of the stator, which makes the winding manufacturing process more challenging.

A. Design Parameters

All the considered designs have the same ten-pole surface permanent magnet (SPM) rotor. Target application is for a 30krpm machine with >120Nm, >140kW and >12krpm base speed. Further constraints for the geometry were stator outer diameter of <140 mm, stator bore diameter of <90 mm and active stack length of 85 mm, as reported in Table II. In addition to these geometrical constraints, the following constructive and applications restrictions where applied:

1. The DC bus voltage is 650Vdc.
2. The inverter phase current rating is 370Arms.
3. Wire fill factor of 65% (copper + insulation)
4. Windings sized for the same Joule loss at peak current.

With these constraints, the main geometric and electric parameters are presented in Tab. II.

Table II – Geometric and electric design parameters

Slot / Pole	**9s/10p**	**12s/10p**	**15s/10p**	**20s/10p**
Tooth width / Stator yoke / Slot depth (mm)	13 / 6.5 / 16.4	10 / 7.3 / 15.6	10.2/5.4 / 17.5	6.4 / 6.3 / 16.6
Winding area (mm2) **Wire area (mm2)**	278 178	194 123	150 96	126 82
Series coil turns per phase	32	32	32	48
Ph resistance @ 200°C (mOhm) **Copper loss @ 370A (kW)**	45 18.5 kW			68 18.6 kW
Winding factor	0.957	0.943	0.866	1

B. Winding factor

The winding factor represents the proportion for which each winding unit contributes to the phase back-emf, and it can be calculated as the vectorial sum of the back-EMF of each winding unit for each phase as:

$$k_w = \frac{|\sum_{i=1}^{Q} n_{c,ph}^{i} \cdot e^{j\alpha_s^e \cdot (i-1)}|}{\sum_{i=1}^{Q} |n_{c,ph}^{i}|} \quad (1)$$

where n_c^i is the number of conductors of the i^{th} slot for one phase and $\alpha_s^e = \frac{2\pi}{Q} \cdot p$ is the electrical angle displacement of each slot.

It has a direct relation with the average electromagnetic torque of the machine as, for a SPM fed with sinusoidal currents, it can be expressed as given by (2) [10].

$$T = \frac{1}{4\pi} k_w n_c Q B A_g \hat{I}_q \quad (2)$$

where k_w is the fundamental winding factor, n_c is the number of conductors per slot, Q is the number of slots, B is the peak value of the fundamental no-load air gap flux density, $A_g$is the air gap area, $\hat{I}_q$ is the peak value of the current in quadrature with the phase of the magnets. This expression does not consider any contribution of reluctance torque, which holds true for the SPM rotor.

III. TWO PHASE INVERTER

For the 3-phase machines, a standard 3-phase voltage source inverter is considered. For the 20s10p bi-phase machine, a 4-leg inverter is considered as per Fig. 2. In this case, each motor phase has a phase voltage range of plus-minus V_{dc} instead of $\frac{V_{dc}}{\sqrt{3}}$ as per the three-phase counterpart, at the cost of one extra inverter leg. Fixed the dc-link voltage and the maximum phase current· I_{max}, the power increment associated to the 4-leg inverter can be understood as:

$$\frac{P_{m,2\phi}}{P_{m,3\phi}} = \frac{\frac{2}{2} \cdot V_{dc} \cdot I_{max} \cdot \eta \cdot PF}{\frac{3}{2} \cdot \frac{V_{dc}}{\sqrt{3}} \cdot I_{max} \cdot \eta \cdot PF} = \frac{2}{\sqrt{3}} \quad (3)$$

Where η and PF are the efficiency and power factor of the 2- and 3-phase machines at peak power conditions, considered equal for ease of comparison. Under such an assumption, a bi-phase machine with the same inverter current rating benefits from a 15.5% power increase. The disadvantages are the increased complexity and cost of adding a fourth leg to the inverter.

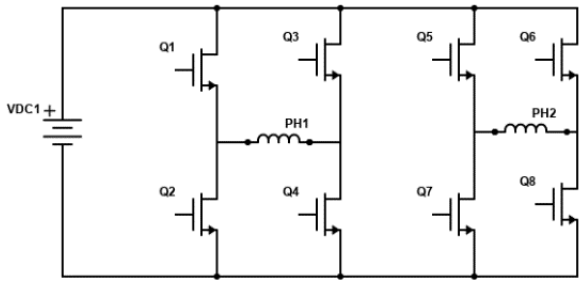

Figure 2. 4-leg inverter for the 20s10p electric machine.

IV. FEM BASED COMPARISON

FEM simulation was performed for the four cases under study. Fig. 4 presents electromagnetic torque for all studied combinations. It shows that 20s10p machine outperforms in

peak torque and power all other slot-pole combinations.

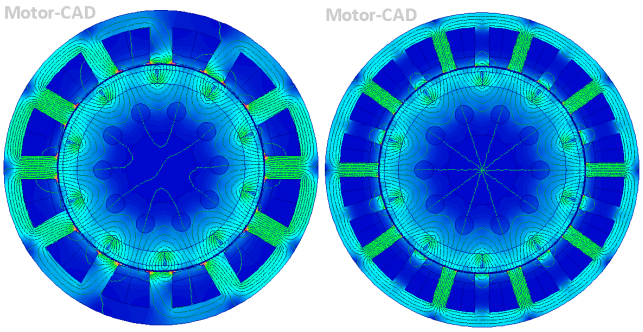

Figure 3. Open Circuit FEM example. Left: 12s10p. Right: 20s10p.

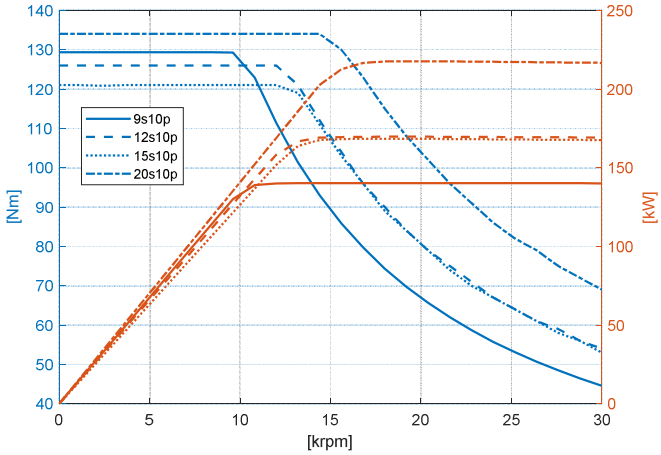

Figure 4. Peak performance results at 650Vdc for all configurations.

Table III presents a summary of peak performance results. The 20s10p machine presents an increase of 28% of peak power (1 over 0.78) with respect to the 12s10p. In addition, peak torque also improved in a similar trend because of the winding factor increase. However, torque ripple is very high and frequency low for the 20s10p with respect to other combinations. This is because torque ripple frequency with respect to mechanical frequency is calculated as the Least Common Multiple between slot and pole number.

Finally, it can be seen as well that 9s10p machine has a lower corner speed. This is mainly because for such winding presents very high q axis flux linkage with respect other combinations.

A. Loss comparison and efficiency map

Copper, Iron and magnet loss have been simulated using FEM. Fig. 5 presents total losses, the sum of these contributes, for two speeds. For the same torque output, the 20s10p machine is more efficient at high loads as, for example, at 126 Nm the 12s10p machine dissipates 19.5kW and the 20s10p 16.8kW, 13% less of total losses. The main contribution to this effect is that for the same torque less current is needed for the 20s10p, as it has a higher winding factor. On the other hand, we see that for low torque values and higher speeds iron losses are slightly higher in the 20s10p than the 12s10p. Fig. 6 and 7 presents the efficiency map for 20s10p and 12s10p machines.

Table III – Peak performance summary

Slot / Pole	9s / 10p	12s/10p	15s/10p	20s/10p
Peak Torque (Nm)	129	127	121	135
Peak Power (kW)	140	169	168	217
Corner speed (rpm)	9.600	12.000	12.000	14.400
Normalized torque	0.96	0.94	0.90	1
Normalized power	0.64	0.78	0.77	1
Pk-pk Torque Ripple (Nm)	2.3	1.4	9.2	24
Torque Ripple Frequency vs. Mech. Frequency	90x	60x	30x	20x

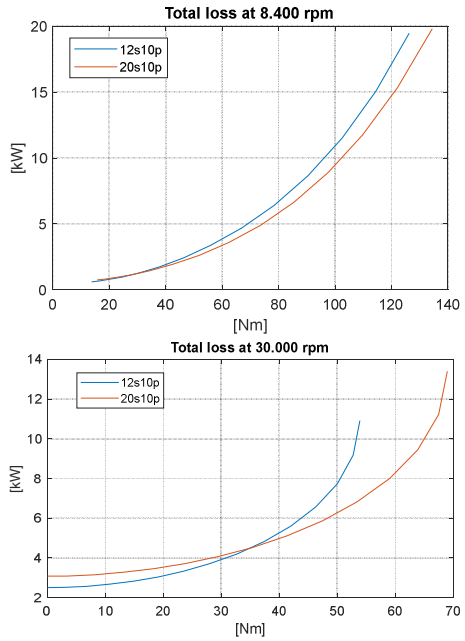

Figure 5. Losses comparison between 20s10p and 12s10p for 2 speeds

V. SIMPLIFIED VIBROACOUSTIC STATOR MODEL

A simplified vibroacoustic model from chapter 6 of [8] has been used to compare the different geometries' noise emissions. This model does not have the intent to determine precise absolute value of noise emission, but it is employed to compare different designs only. The main assumptions for the model are the following:

A. Stator is the main source of noise.
B. Stator is modeled as an infinite long cylindrical radiator, simplified with a homogeneous material of radius r_{eq}, length L_{eq}, thickness h_{eq} and density ρ_{eq}, es per Fig.7.
C. Main source of excitation comes from radial electromagnetic forces.
D. Only circumferential modes of are considered, so the force component of order "r" only excites the mode of the same order for the stator.

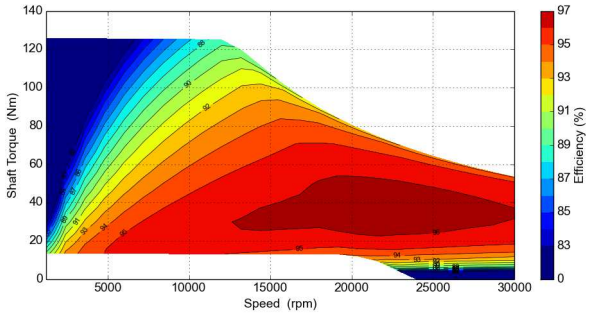

Figure 6. Two phase 20slot-10pole efficiency map

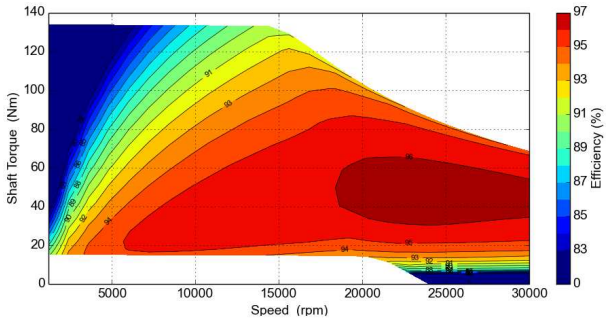

Figure 7. Three phase 12slot-10pole efficiency map

Assumption "A" holds true for many radial flux automotive applications as rotor vibration modes are usually higher than the stator. Cases in which rotor noise emissions can be higher than stator are in axial flux electrical machines, where the rotor plate can be excited and produce significant noise for specific speed ranges. Assumption "C" can be overcome by incorporating tangential forces into the analytical model, however they are usually much lower than radial forces for a radial machine. Assumptions "B" and "D" consider the stator as an infinite cylinder, which as its length becomes shorter it can be expected that the end effects would become more significant and the results from the model less representative. However, the aim is not to catch the exact values of noise, rather than predict a trend to compare different architectures.

Fig. 9 presents some examples of the first 4 radial modes of deformation for the equivalent cylinder. As presented in [3], these modes are excited mainly by the lowest radial force harmonic order, which for fractional slot machines is the greatest common divider of Q and $2p$.

Table IV – Lowest radial force order for studied machines

Slot / Pole Combination	**9s / 10p**	**12s / 10p**	**15s / 10p**	**20s/10p**
Lowest spatial radial force order	1	2	5	10

Sound power (Π) radiated from the structure, in Watt, is calculated as the sum of power radiated from each vibration mode ($\Pi_{m,n}$) as per Eq. (4).

$$\Pi = \sum_m \Pi_m = \sum \rho_0 c_0 S \langle \bar{v}_m^2 \rangle \sigma_m \qquad (4)$$

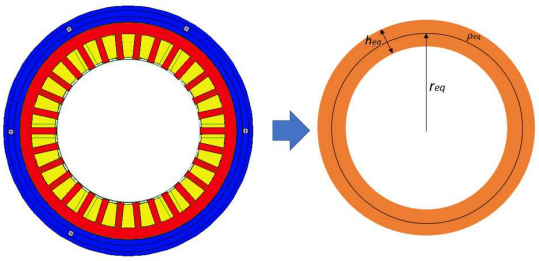

Figure 8. Equivalent stator model

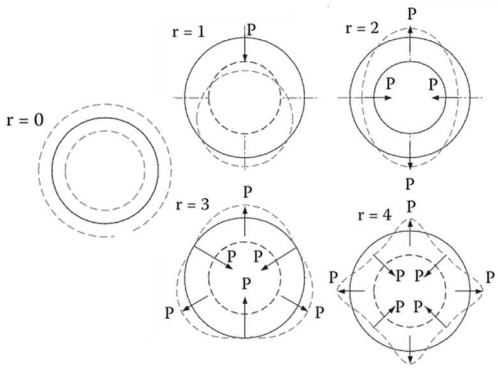

Figure 9. Deformation of core caused by space distribution of radial forces. Source [8].

Where ρ_0, c_0 are the density and the sound speed in the ambient medium, S is the area of the radiating surface, $\langle \bar{v}_{m,n}^2 \rangle$ is the spatial averaged mean square velocity of the mth spatial mode and nth time mode and σ_m is the modal radiation efficiency for the mth spatial mode.

Then sound power level indicator (dB) is defined as Eq.(5), compared as to the reference power 10^{-12} Watts, which is the lowest sound persons can discern.

$$SWL = 10\, log\left(\frac{\Pi}{10^{-12}}\right) \qquad (5)$$

The modal radiation efficiency $\sigma_m(m, k_0 r_{eq})$ depends on the mode, the radius r_{eq} and the wave number k_0 of the specific cylinder mode, as presented in Eq. (6.44) of [8].

The mean square velocity of the surface vibrating at mode m with radial forces of time order n is calculated as Eq. (6).

$$\langle \bar{v}_m^2 \rangle = \frac{V_{m,n}^2}{4\pi} \int_0^{2\pi} cos(m\theta)\, d\theta \qquad (6)$$

Where $V_{m,n}$ is radial velocity amplitude of mode m at angular frequency. Finally, the amplitude of the vibration velocity for mode m can be calculated as per Eq. (7).

$$V_m = 2\pi f_r \frac{2\pi r_{eq} L_{eq}}{M \omega_m^2} h_m P_{mr} \qquad (7)$$

Where f_r is the frequency of the electromagnetic force of order r, M is the mass of the cylindrical shell ω_m is the angular natural frequency of the mode m, h_m is the magnification factor as per Eq. (8), and P_{mr} is the magnetic pressure magnitude obtained from radial force spectral amplitude as per Eq. (9). Damping factor ξ_m on stator depends on damping sources (material damping as potting or glue, or friction

damping as friction between lamination sheets or wires). Its value can be estimated experimentally from free-free modal analysis of the stator, and its value ranges from 0.5% to 4%. For the following calculations a typical value of 1% is used.

$$h_m = \frac{1}{\sqrt{\left(1-\left(\frac{f_r}{f_m}\right)^2\right)^2 + (2\xi_m\left(\frac{f_r}{f_m}\right))^2}} \quad (8)$$

$$P_{mr} = \frac{|F_r|}{l_{eq} 2\pi r_{eq}} \quad (9)$$

A. *Radial Forces and sound power*

Radial forces have been FEM calculated for the four machines under open circuit and load conditions. As an example, space-time harmonics are presented in Fig. 10 for the 12s10p machine, where the second space order is the main candidate to contribute to noise at 10th mechanical order frequency.

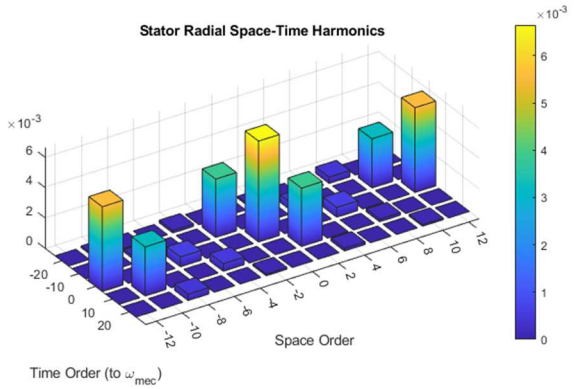

Figure 10. Space and time order (time with respect to mechanical frequency) radial force harmonics

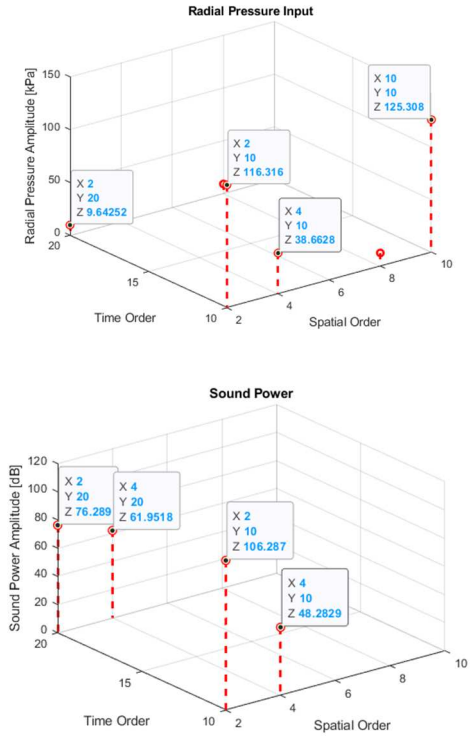

Figure 11. Simulation output for 12s10p configuration. Up: Radial Pressure Input. Down: Sound Power Amplitude. (X axis: Spatial Order. Y axis: Time Order w.r.t mech. frequency. Z axis: Sound Power Amplitude)

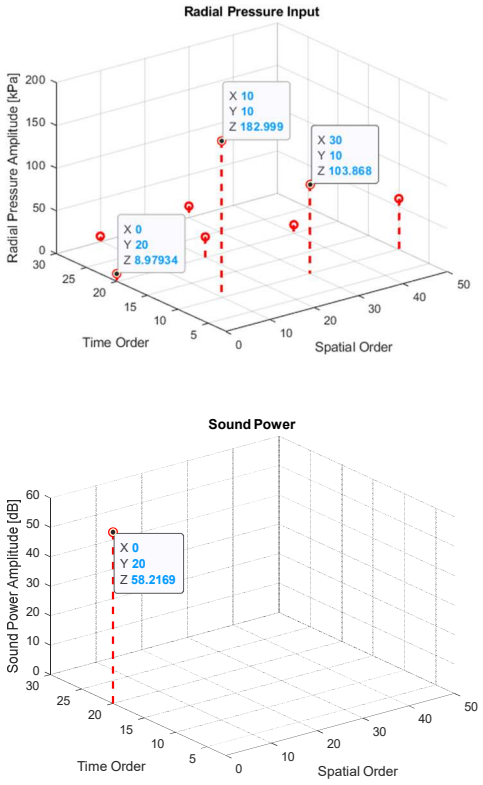

Figure 12. Simulation output for 20s10p configuration. Up: Radial Pressure Input. Down: Sound Power Amplitude. (X axis: Spatial Order. Y axis: Time Order w.r.t mech. frequency. Z axis: Sound Power Amplitude)

Fig. 11 presents the output from the simplified vibroacoustic model for the 12s10p at a maximum torque operation at 8000 rpm, where overall sound power is 106 dB. Spatial orders 2 and 4 contribute to the sound power, where the 2nd dominates over the 4th. The higher 10th spatial order does not have significant effect on sound power though developing the highest radial pressure amplitude. The time order follows the pole number leading to a frequency of 1.3 kHz at 8000 rpm. This is well within the hearable sound frequency band.

Fig. 12 presents the output from the simplified vibroacoustic model for the 20s10p at same speed and maximum load condition. The sound power level is 58 dB, which is a -48 dB reduction with respect to the same condition of the 12s10p. The main contribution to sound power in this case is zeroth mode at 20 times the mechanical frequency, 2.6 kHz in this case.

Table V summarizes the output of the simplified vibroacoustic model for all studied machine combinations. It shows that the 20s/10p machine is the best slot/pole combination and the 12s/10p the worst, generating as much as 106 dB of SPL at load, which is impractical for any automotive application.

VI. Conclusions

The proposed two phase machine is an alternative for very high power density applications as, for the same volume, power performances are increased 28% with respect to the 12s10p next best solution. In addition, it presents a significantly lower noise emission, as sound power is -48 dB with respect to the same machine at 8.000 rpm and peak torque. These noise level results were obtained with a simplified analytical NVH model. In future work, the 12s10p and 20s10p architectures will be compared using an NVH FEM model. Last, the 20s10p machine presents construction challenges, as windings are overlapped and not modular. Also, torque ripple is substantial (17% of maximum torque vs 1% of the 12sp10), to be further optimized by detailed electromagnetic design.

Table V – Sound Power Level

Slot / Pole	9s / 10p	12s / 10p	15s / 10p	20s/10p
Open Circuit RMS sound power. 8000 rpm	63 dB	100 dB	45 dB	< 20 dB
On Load RMS sound power level at 8000 rpm	89 dB	106 dB	58 dB	58 dB

VII. Acknowledgment

The authors gratefully acknowledge the contributions of M. Gamba, S. Pasquale, D. Ferrara and P. Faverzani for their work on the original version of this document. This research has been conducted with the support of the Power Electronics Innovation Center (PEIC) of Politecnico di Torino.

References

[1] Z. Q. Zhu, Z. P. Xia, L. J. Wu and G. W. Jewell, "Influence of slot and pole number combination on radial force and vibration modes in fractional slot PM brushless machines having single- and double-layer windings," 2009 IEEE Energy Conversion Congress and Exposition, 2009, pp. 3443-3450, doi: 10.1109/ECCE.2009.5316553.

[2] T. Sun, J. -M. Kim, G. -H. Lee, J. -P. Hong and M. -R. Choi, "Effect of Pole and Slot Combination on Noise and Vibration in Permanent Magnet Synchronous Motor," in IEEE Transactions on Magnetics, vol. 47, no. 5, pp. 1038-1041, May 2011, doi: 10.1109/TMAG.2010.2093872.

[3] H. Yang and Y. Chen, "Influence of Radial Force Harmonics With Low Mode Number on Electromagnetic Vibration of PMSM," in IEEE Transactions on Energy Conversion, vol. 29, no. 1, pp. 38-45, March 2014, doi: 10.1109/TEC.2013.2290304.

[4] K. Wang, Z. Q. Zhu, L. J. Wu and G. Ombach, "Comparison of electromagnetic performance of 2- and 3-phase PM brushless AC machines for low speed applications," 6th IET International Conference on Power Electronics, Machines and Drives (PEMD 2012), Bristol, 2012, pp. 1-6, doi: 10.1049/cp.2012.0280.

[5] F. Zürcher, T. Nussbaumer, W. Gruber, and J. W. Kolar, "Comparison of 2- and 3-phase bearingless slice concepts," *Journal of System Design and Dynamics*, vol. 3, no. 4, pp. 471-482, 2008.

[6] J. Chai, J. Wang, K. Atallah and D. Howe, "Performance Comparison and Winding Fault Detection of Duplex 2-Phase and 3-Phase Fault-Tolerant Permanent Magnet Brushless Machines," 2007 IEEE Industry Applications Annual Meeting, New Orleans, LA, USA, 2007, pp. 566-572, doi: 10.1109/07IAS.2007.91.

[7] T. Stoyanov and R. Spasov, "Analysis of Two-phase Permanent Magnet Synchronous Machines Used for Hybrid Vehicles," 2018 10th Electrical Engineering Faculty Conference (BulEF), Sozopol, Bulgaria, 2018, pp. 1-3, doi: 10.1109/BULEF.2018.8646932.

[8] W. Zhao, T. A. Lipo and B. Kwon, "Dual stator two-phase permanent magnet machines with phase-group concentrated-coil windings for torque enhancement," 2015 IEEE International Magnetics Conference (INTERMAG), Beijing, China, 2015, pp. 1-1, doi: 10.1109/INTMAG.2015.7156638.

[9] Yue Li, T. A. Walls, J. D. Lloyd and J. L. Skinner, "A novel two-phase BPM drive system with high power density and low cost," in IEEE Transactions on Industry Applications, vol. 34, no. 5, pp. 1072-1080, Sept.-Oct. 1998, doi: 10.1109/28.720447.

[10] Gieras, J.F., Wang, C., & Lai, J.C. (2006). Noise of Polyphase Electric Motors (1st ed.). CRC Press. https://doi.org/10.1201/9781420027730

[11] Z. Q. Zhu, Z. P. Xia, L. J. Wu and G. W. Jewell, "Influence of slot and pole number combination on radial force and vibration modes in fractional slot PM brushless machines having single- and double-layer windings," 2009 IEEE Energy Conversion Congress and Exposition, 2009, pp. 3443-3450, doi: 10.1109/ECCE.2009.5316553.

[12] F. Magnussen and C. Sadarangani, "Winding factors and Joule losses of permanent magnet machines with concentrated windings," IEEE International Electric Machines and Drives Conference, 2003. IEMDC'03., 2003, pp. 333-339 vol.1, doi: 10.1109/IEMDC.2003.1211284.

Biographies

M. F. Troncoso C, born in Chile in 1988, received the MSc in electrical engineering from Politecnico di Torino, Turin, Italy in 2013 in a double degree with Pontificia Universidad Catolica de Chile (PUC). Received professional title in industrial engineering with focus in electrical engineering from PUC also in 2013 in Chile.

He is currently performing an industrial PhD at the Power Electronics Interdepartmental Laboratory (PEIC) at Politecnico di Torino, for an automotive company in Italy. He worked in Coener in the field of renewable energies. performed laboratory courses in PUC and co-founded the start-ups RT Electronics and Reborn Electric in Chile. Now works in Italy for an automotive company in the field of testing components for hybrid vehicles applications.

Fausto Stella (M'18) received the B.Sc. and M.Sc. degrees in electrical engineering from the Politecnico di Torino, Turin, Italy in 2012 and 2015, respectively. He was a visiting Ph.D. student at the University of Nottingham, U.K. and in 2019 he received the Ph.D. degree from the Politecnico di Torino, He is currently an Assistant Professor with the Politecnico di Torino. His research interests include the design of power electronic converters, focusing on SiC semiconductors and reliability issues, and the control of converters via embedded systems.

Gianmario Pellegrino (M'03, SM'13, F'22) received the MSc and PhD degrees in electrical engineering from Politecnico di Torino, Turin, Italy in 1998 and 2002, respectively. He is currently a Professor of Power Converters, Electrical Machines and Drives at the same university. Dr. Pellegrino is engaged in several research projects with the industry, and one of the authors of the open-source project SyR-e for the design of electrical motors and drives. He was a visiting fellow at Aalborg University, DK, the University of Nottingham, UK, and the University of Wisconsin-Madison, USA. Dr. Pellegrino is an Associate Editor for the IEEE Transactions on Industry Applications and has 55+ IEEE journal papers, three patents and nine Best Paper Awards. He is a member of the Power Electronics Interdepartmental Laboratory (PEIC) established in 2017 at the Politecnico di Torino and a member of the Advisory Board of PCIM (Power Conversion and Intelligent Motion) Europe. He is currently the Rector's Advisor for Interdepartmental Centres of Politecnico di Tori